

PAPER

Resonance enhancement of harmonics in the vicinity of 32 nm spectral range during propagation of femtosecond pulses through the molybdenum plasma

To cite this article: V V Kim *et al* 2020 *J. Phys. B: At. Mol. Opt. Phys.* **53** 195401

View the [article online](#) for updates and enhancements.








IOP | ebooks™

Bringing together innovative digital publishing with leading authors from the global scientific community.

Start exploring the collection—download the first chapter of every title for free.

Resonance enhancement of harmonics in the vicinity of 32 nm spectral range during propagation of femtosecond pulses through the molybdenum plasma

V V Kim^{1,7}, G S Boltaev^{1,2}, M Iqbal¹, N A Abbasi¹, H Al-Harmi¹, I S Wahyutama^{3,7,8} , T Sato^{3,4,5} , K L Ishikawa^{3,4,5} , R A Ganeev^{1,6,9}  and A S Alnaser¹ 

¹ Department of Physics, American University of Sharjah, PO Box 26666, Sharjah, United Arab Emirates

² Tashkent Institute of Irrigation and Agricultural Mechanization Engineers, Tashkent 100000, Uzbekistan

³ Department of Nuclear Engineering and Management, Graduate School of Engineering, The University of Tokyo, 7-3-1 Hongo, Bunkyo-ku, Tokyo, 113-8656, Japan

⁴ Photon Science Center, Graduate School of Engineering, The University of Tokyo, 7-3-1 Hongo, Bunkyo-ku, Tokyo 113-8656, Japan

⁵ Research Institute for Photon Science and Laser Technology, The University of Tokyo, 7-3-1 Hongo, Bunkyo-ku, Tokyo 113-0033, Japan

⁶ Faculty of Physics, Voronezh State University, Voronezh 394018, Russia

E-mail: rashid_ganeev@mail.ru

Received 13 April 2020, revised 23 June 2020

Accepted for publication 13 July 2020

Published 25 August 2020



Abstract

We demonstrate the enhancement of harmonics in the vicinity of 32 nm while generating them in the Mo laser-produced plasma. The enhanced harmonics centered at around the 25th harmonic of 806 nm radiation were analyzed by different means (delay between heating and driving pulses, dependences of harmonic yield on the driving and heating pulse intensities and durations, different regimes of plasma formation, two-color pump of plasma, application of chirped pulses, etc). The role of strong ionic transition possessing large oscillator strength leading to the growth of the nonlinear optical response is discussed. Comparative studies using molybdenum, silver, and chromium laser-produced plasmas are presented. To validate the experimental findings, we numerically simulate harmonic generation from Mo using full-dimensional, all-electron, first-principles calculations. The calculated harmonic spectra exhibit a prominent peak around 32 nm and a suppression around 36–38 nm, successfully reproducing the experimentally observed features. Our transition-resolved analyses of the calculation results reveal both that the $4p$ - $4d$ transitions are responsible for the observed enhancement and that the destructive interference between the $4p$ - $4d$ transitions and the recombination to the $4d$ orbitals leads to the observed suppression.

Keywords: molybdenum plasma, high-order harmonics, resonance enhancement

(Some figures may appear in colour only in the online journal)

⁷ These authors equally contributed to this work.

⁸ Present address: Louisiana State University, Baton Rouge, LA 70803-4001, United States of America.

⁹ Author to whom any correspondence should be addressed.

1. Introduction

The development of effective sources of coherent extreme ultraviolet (XUV) radiation is important for the fundamental and practical needs of optics. The high-order harmonics generation (HHG) of ultrashort laser pulses in isotropic media (gases [1] and preformed laser plasma [2]) is the simplest and most reliable method of changing the frequency of exciting pulses in the XUV direction. Methods of HHG enhancement include optimization of various parameters, such as particle density and excitation level, intensity of exciting pulses, fluence of HP, etc, to create preferred conditions of this process, when phase mismatch does not play a decisive role in limiting the HHG conversion efficiency.

Various metals, metal alloys, insulators and semiconductors were previously analyzed by ablation and HHG in laser-produced plasmas (LPP) [3–15]. A number of studies have demonstrated higher conversion efficiency in LPP compared to gases [16, 17]. Further optimization of this process involves the application of various methods that cannot be implemented in the case of HHG in gases. These include the use of relatively large aggregates (quantum dots and nanoparticles [5, 18]), the implementation of resonance amplification of single harmonic and the formation of specific conditions of modulated LPP, when quasi-phase matching is achieved for different groups of harmonics. Some other methods that are also applicable for HHG in gases include the two-color medium pump, the application of few- and multi-cycle pulses, the use of mid-infrared lasers and extended media [8, 16, 17], etc can also lead to an increase in harmonic output. All these amendments are difficult to implement in a single experiment, as some requirements for these methods contradict each other. Under any optimal conditions, the low concentration of active harmonic sources (atoms, ions, multiparticle species), when considered in comparison with the solid state, significantly limits the conversion efficiency of harmonic generation. Studies of this process in solids [19] have shown some advantages and disadvantages, while limiting the spectral region of generation to the absorption edge of the solid materials used. Thus, the search for new methods, schemes, materials and approaches is of paramount importance for the improvement of HHG.

One of the above methods is related to the search for the resonant amplification of some harmonics located near the ionic transitions, which have a large oscillator strength. Theoretical approaches to the description of resonant HHG were presented in [20–33]. Indium, tin, chromium, manganese, and arsenic were among those species that, when ablated and interacting with a propagating laser pulse, demonstrated amplification of some harmonic orders of widely used Ti:sapphire lasers [34–36]. The search for plasma components that allow such amplification is an important task of nonlinear optics.

One of potential candidates for the enhancement of harmonics in the XUV range is a plasma produced on the surface of molybdenum. This transition metal forms chemical compounds in oxidation states. The plasma characteristics of pure molybdenum targets irradiated with 2 ns, 300 mJ pulses from an Nd:YAG laser at its second harmonic wavelength of 532 nm were reported in [37]. The temperature of the plasma and

electron density were analyzed at different delays from the beginning of ablation. Those studies were carried out in the visible range of plasma emission. Meanwhile, there are still no, to the best of our knowledge, reports of the strong transitions of molybdenum in XUV range. Notice that HHG studies of some transition metals have shown the existence of XUV transitions possessing strong oscillator strength, which can be considered as a method for the nonlinear optical spectroscopy of atoms and ions. A search for such transitions in the case of Mo laser-produced plasma through harmonics generation can reveal the advantages in the application of this technique for atomic and plasma physics. The importance of these studies is justified by the applications for the analysis of, for instance, the resonance processes in atomic and molecular plasmas.

In this paper, we analyze these processes using the femtosecond pulses propagating through the Mo plasma. We demonstrate the resonant 25th harmonic amplification in the vicinity of 32 nm when femtosecond pulses propagate through the plasma generated from a molybdenum target. We analyze the amplified 25th harmonic of 806 nm radiation using various methods to optimize this process. The role of a strong ion transition with a large oscillator strength leading to an increase in the nonlinear optical response is discussed.

2. Experimental arrangements

Femtosecond laser pulses (806 nm, 50 fs, 10 Hz) from Ti:sapphire laser were used for HHG during propagation of this radiation through Mo-containing laser plasmas. For delay-dependence studies, we used a scheme to heat the target by nanosecond pulses and excite LPP by femtosecond pulses. In that case, the ablation of the target was carried out using the Nd:YAG laser (1064 nm, 10 ns, 10 Hz). The driving femtosecond pulses propagated 0.3 mm above the surface of the ablated target (figure 1). We also used the near infrared pulses (1300 nm, 1.3 mJ, 70 fs, 10 Hz) from the optical parametric amplifier (OPA) [38] as the driving radiation and its second harmonic emission to compare HHG in Mo LPP using the pulses of different wavelengths. A $5 \times 5 \times 2$ mm³ molybdenum plate (>99%, Sigma-Aldrich) was inserted into the vacuum chamber.

The delay between nanosecond HP and femtosecond DP was maintained and varied using an electronic delay generator. We also used picosecond pulses from a Ti:sapphire laser by isolating a portion of uncompressed radiation with a pulse duration of 370 ps and a pulse energy up to 2 mJ to ablate the Mo target. The maximal harmonic yield was obtained at 150 ns delay between the heating (pico- and nanosecond) and driving (femtosecond) pulses. Harmonic radiation was analyzed using XUV spectrometer consisting of a vertical slit, a cylindrical mirror with a gold coating, a flat field grating of 2400 lines mm⁻¹, a microchannel plate and a CCD camera.

The most important parameters in the study of HHG plasma are the fluence of the HP and the intensity of the DP. The fluence of nanosecond and picosecond HP on the target surface was 15 and 1.5 J cm⁻², respectively, depending on the studied harmonic generation conditions. The difference in the optimal fluencies allowing the strongest emission of harmonics is

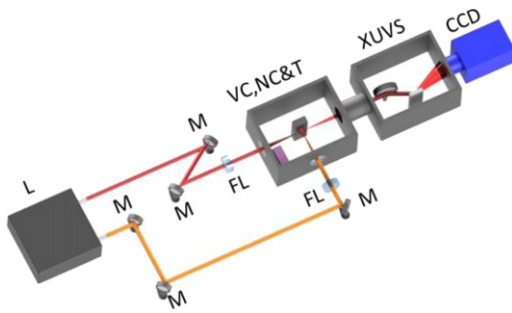


Figure 1. Experimental setup for HHG in Mo LPP. L, femtosecond laser; M, mirrors; FL, focusing lenses; VC, NC and T, vacuum chamber, nonlinear crystal and target. XUVS, extreme ultraviolet spectrometer; CCD, CCD camera.

attributed to different conditions of plasma formation during ablation of Mo bulk target. The intensity of the driving 806 nm pulses did not exceed $4 \times 10^{14} \text{ W cm}^{-2}$. Higher intensities of DP caused strong plasma excitation and a decrease in harmonic output, probably due to the appearance of a large concentration of free electrons leading to phase mismatch between the harmonic and driving waves.

HHG was performed using a single-color pump (SCP) or two-color pump (TCP) of plasma to determine the highest harmonic yield in different XUV ranges. For TCP, the fundamental radiation at 806 nm and 1300 nm and their second harmonics were used. A 0.3 mm thick barium borate (BBO) crystal was installed inside the vacuum chamber along the path of the 806 nm or 1300 nm radiation to generate the second harmonic. The conversion efficiency of the second harmonic pulses was $\sim 3\%$.

3. Results

We chose the conditions of Mo LPP formation when plasma emission became suppressed so that no incoherent radiation was observed alongside the harmonic emission using both picosecond and nanosecond HP. Particularly, this regime of HHG was maintained at 2 J cm^{-2} fluence of heating 200 ps pulses. The heating of Mo target at 5 J cm^{-2} fluence led to appearance of strong plasma emission in the 15–90 nm spectral range and the significant decrease of harmonic emission. Earlier, low-order harmonics generating from Mo plasma in the 3–14 eV range have demonstrated a fast decrease of harmonic yield between 3rd and 9th orders, with the ratio of these harmonic yields 200:1 [39]. Our present studies were extended in the shorter wavelength range (up to 35 eV), which showed a gradual decrease of each harmonic order corresponding to the plateaulike distribution of harmonic intensities between H11 and H19.

Our studies of HHG in Mo plasma started with the analysis of the role of the delay between the heating 10 ns, 1064 nm pulses and the driving 50 fs, 806 nm pulses in variations of the harmonic spectrum. The optimal delay between HP and DP depends on the velocity of the plasma plume containing Mo species (atoms and ions) and the distance between the target surface and the axis of propagation of the DP. One has

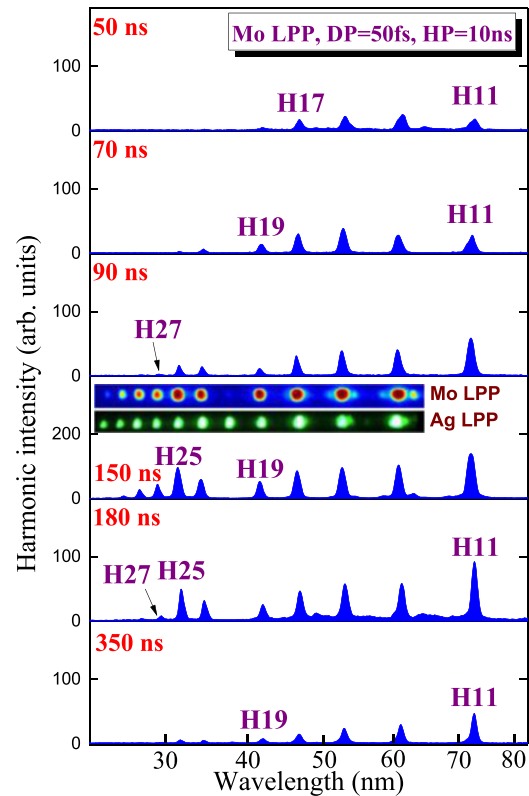


Figure 2. Harmonic spectra from the Mo LPP produced by heating nanosecond pulses (HP) at optimal fluence of heating radiation and SCP using 806 nm, 50 fs driving pulses (DP). The spectra were collected at different delays between HP and DP (20–800 ns; in the graphs we show the 50–350 ns range of delays, from top to bottom). The maximal yield was observed at 150 ns delay. The insets in the fourth panel show the raw saturated images of harmonics generated from molybdenum and silver plasmas.

to choose the conditions when the driving pulse propagates through the densest part of plasma cloud. Commonly, these delays become equal to 50–200 ns depending on the atomic weight of the ablated target. The application of the optical delay, which implies the formation of long optical path (of the order of a few tens meters) for the driving femtosecond pulse, in most cases becomes impractical especially in the case of high-mass atoms belonging to the second half of periodic table. Because of this we used electronically synchronized lasers (Ti:sapphire and Nd:YAG), which allowed fine tuning of the delay between pulses from these laser sources in the range of 0 to a few tens of microseconds by using the digital delay generator. At these conditions, the formation of plasma by nanosecond laser and propagation of pulses from femtosecond laser can be properly synchronized with each other.

The harmonics were observed in a broad range of 20 to 800 ns delays. Figure 2 depicts the harmonic spectra produced from the Mo plasma during ablation by 10 ns pulses at 50–350 ns delays between the nanosecond and the femtosecond pulses. At delays smaller than 50 ns the concentration of plasma along the optical axis of driving pulse propagation is still too low to generate strong harmonics. Then, with the growth of delay, the harmonic yield steadily increases until achieving the maximal values at 150 ns delay (fourth panel from the top). Further

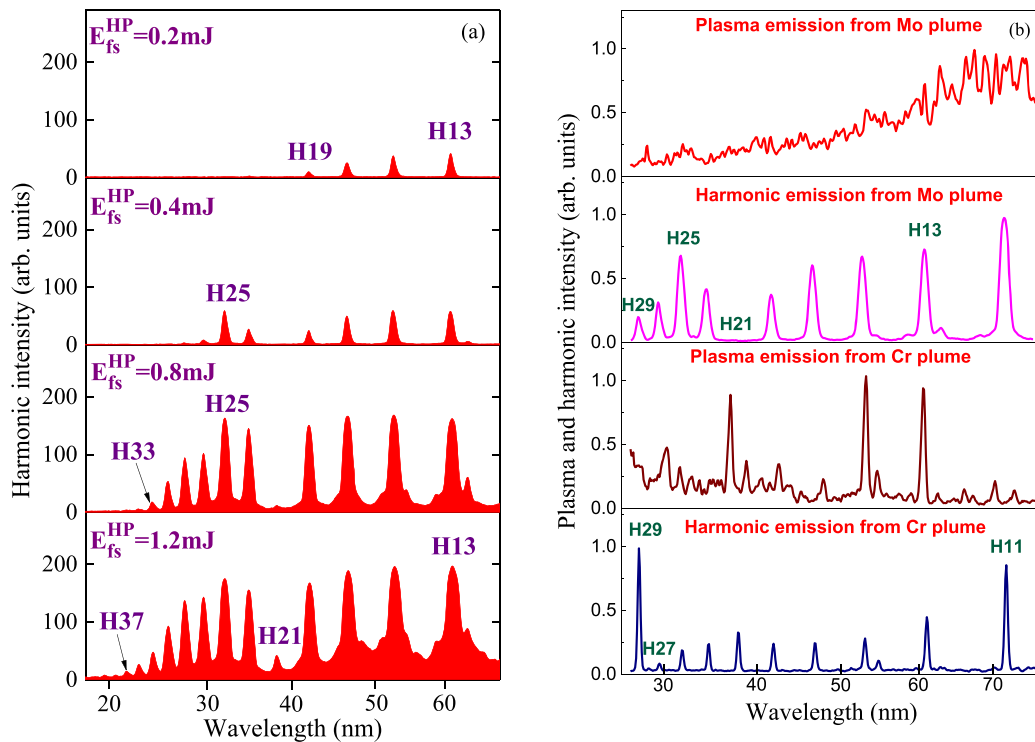


Figure 3. (a) Harmonic spectra from the Mo plasma produced by 370 ps pulses. The spectra were collected at different energies of HP (0.2–1.2 mJ from top to bottom). The maximal yield of odd harmonics was observed at the 0.8 mJ energy of HP. Further growth of heating pulse energy led to a decrease of HHG conversion efficiency. (b) Plasma (upper panel) and harmonic (second panel) spectra from ablated Mo target. No specific emission lines and absorption bands were observed in the vicinity of enhanced 25th harmonic and suppressed 21st harmonic, respectively. Two bottom panels show the plasma and harmonic spectra from ablated Cr target where the enhanced 29th harmonic was observed.

growth of delay causes a gradual decrease of harmonics until entire disappearance at the delays larger than 800 ns. One can estimate the velocity of Mo plasma ($\sim 2 \times 10^3 \text{ m s}^{-1}$) at the used conditions of optimal ablation by nanosecond pulses (fluence 12 J cm^{-2}) by knowing the distance from target surface ($300 \mu\text{m}$) and the time of propagation of this distance by densest area of the cloud of particles spreading out from the target surface (150 ns).

The presence of ions in plasma plume can be characterized by analyzing the emission in the visible and XUV ranges. The plasma emission in the visible range at the used fluence and intensity of the heating radiation mainly consisted of the transitions in Mo I and Mo II (see also [39]). There was no plasma emission observed in the XUV region at these conditions of ablation. The harmonic emission was the only source of XUV radiation at these conditions. The appearance of emission lines in the 30–90 nm range at higher fluencies of heating radiation caused a decrease of harmonic yield due to appearance of the free electrons preventing the maintenance of the optimal phase matching conditions between the interacting waves of harmonic and DP.

The most interesting feature of the spectra shown in figure 2 is a notable heterogeneity of the envelope of harmonic distribution appearing at the delays longer than 90 ns. One can see the entire absence of the 21st harmonic (H21), while H25 becomes stronger than the neighboring ones. Such an unusual pattern of harmonic distribution in the case of Mo plasma has

been observed in [40] without the elaboration of various features of this process. This behavior of harmonic distribution is in contrast with the commonly observable gradual decrease of each next harmonic order until the cutoff region. The example of latter harmonic distribution is shown in the bottom inset of figure 2 where the raw image of harmonic spectrum generated in silver plasma is presented, while the raw image of harmonics from molybdenum plasma is shown in the upper inset. Ag plasma allows, like most of other LPPs, the appearance of all harmonics with approximately similar intensity corresponding to the plateaulike distribution of the harmonics steadily decreasing towards to shorter-wavelength region. These two images are collected at the saturated regime of registration for better visibility of this peculiarity in the difference of harmonic spectra, while the line-outs of harmonic spectra presented in this and other figures were taken from the unsaturated images of harmonics.

Figure 3(a) shows the harmonic spectra from the Mo plasma produced by 370 ps pulses at different energies of HP. The application of picosecond pulses has some attractiveness and disadvantages with regard to the use of nanosecond HP. Here we just notice that the optimal delay in present experiments using 370 ps HP was shifted towards 70 ns once we decreased the distance between the ablating target and femtosecond beam. Overall, the HHG conversion efficiency in the case of picosecond HP was approximately two to three times higher compared with the case of plasma formation using nanosecond

pulses. The harmonic spectra were modified by controlling the energy of HP (0.2–1.2 mJ from top to bottom). The maximal yield of odd harmonics was observed at the 0.8 mJ energy of heating picosecond pulses. The growth of heating pulse energy led to a saturation and further decrease of HHG conversion efficiency. Particularly, in the case of 1.8 mJ, 370 ps pulses we observed the notable (i.e. approximately three to five times) decrease of harmonic yield and increase of plasma emission, alongside with the disappearance of the resonantly-enhanced group of harmonics centered at around of $\lambda = 32$ nm.

The origin of such an unusual spectral shape of harmonics from Mo plasma shown in figures 2 and 3(a) is attributed to the influence of the ionic transition in the vicinity of 32 nm possessing large oscillator strength. Similar effect has earlier been reported during experiments with a few other plasmas produced on the surfaces of some metals, like In, Cr, Sn, and Mn [35, 36, 41, 42]. The theoretical explanation of this effect is given in [28] using the developed four-step model of HHG at resonance conditions. Increasing the harmonic yield in the vicinity of resonances introduces a new possibility of increasing the conversion efficiency of a certain harmonic order. Such a unique source of radiation would be ideal to accelerate its various applications in physics, chemistry, and biology, and explore new areas such as nonlinear x-rays optics and attosecond physics.

We did not find in the literature data on the strong ionic transitions of Mo in the vicinity of 32.2 nm, which corresponded to the H25 of 806 nm radiation. No information is available on the oscillator strengths of the Mo II–Mo IV transitions in this spectral region, to our best knowledge. Actually, only a few transitions of Mo V are reported in this region [43]. The observation of the influence of strong transitions yet reported during studies of Mo plasma emission demonstrates the advantages in the application of HHG as a tool for the nonlinear optical spectroscopy of atoms and ions.

We studied the emission spectra from Mo plasma during over-heating of targets surface (figure 3(b), upper panel) and did not observe the emission of lines in the vicinity of 32 nm, which could be related with the unusual envelope of harmonic spectra (figure 3(b), second panel). Notice that the presence of strong ionic emission lines does not relate to the possibility of the enhanced harmonic generation in this region. In other words, the ionic transitions possessing large oscillator strength does not necessarily correlate with the strong incoherent emission at the wavelength of these transitions. Moreover, the presence of strong emission at some spectral ranges may indicate the unavailability of the conditions for the resonance-induced growth of harmonic yield. The example of such a relation was demonstrated in the case of our studies of the harmonic generation from chromium plasma. Chromium plasma is another example demonstrating the enhancement of single (29th) harmonic of Ti:sapphire laser (figure 3(b), bottom panel). This process has earlier been analyzed in [44]. Some strong transitions associated with the singly charged Cr in the region of 27.3 nm, which is close to the H29 of 806 nm driving radiation, were reported in [45]. Our studies show that this harmonic approximately coincides with the short-wavelength wing of the strong spectral band of the $3p \rightarrow 3d$ transitions of Cr II ions.

Meanwhile, no particularities were observed in the plasma emission spectra from this material at 27.3 nm (figure 3(b), third panel from the top), and vice versa, the closeness of some harmonics (particularly H21) with strong emission lines did not cause their enhancement or suppression.

In some circumstances, the optimal phase conditions can be maintained for a single harmonic, the wavelength of which being located at the shorter side of resonance. The refractive index of the plasma in the vicinity of a resonant transition can be notably modified, which can lead to the matching of the refractive indices of the plasma at the wavelengths of the driving pulse and some harmonic being located in the vicinity of the blue side of resonance due to the anomalous dispersion in this region. Contrary to that, the lower order harmonic can be affected by the growing normal dispersion in the vicinity of the red side of resonance. In that case the phase mismatch notably increases, which leads to the suppression of this harmonic. Such a pattern can qualitatively explain the experimental observation of the significant suppression of H21 and enhancement of H25 in Mo plasma. The intermediate harmonic (H23), which is probably located close to the resonance, does not deviate from the averaged phase matched conditions. One can assume that such resonance conditions do not cause strong absorption of this harmonic. Notice that all above-described studies were performed using SCP of LPP. In this connection, one can assume that application of TCP concept can reveal some additional peculiarities of this process due to larger amount of generating harmonics in the resonance region.

Initially, the application of two waves (i.e. radiation of Ti:sapphire laser and its second harmonic (H2)) interacting in a nonlinear optical medium for improvement of HHG has been introduced during frequency conversion in the gas medium [46–50]. TCP concept allows generating odd harmonics, which are stronger than those with the driving field alone, as well as generating even harmonics as strong as the odd ones, which leads to energy enhancement of the high-order harmonics. Those studies have been experimentally treated using both parallel and perpendicularly linearly polarized two-color fields. The suitable control of the relative phase between the fundamental and H2 radiation allows the orthogonally polarized second field participating in the modification of the trajectory of accelerated electron from being two-dimensional to three-dimensional, which may lead to removal of the medium symmetry and generation of equal odd and even harmonics. This approach has been applied for harmonic generation in LPPs as well [51]. In those studies, the driving radiation and its weak H2 (at the energy ratio of 50:1) were linearly polarized orthogonal to each other, similarly to other following studies of plasma TCP HHG [52].

Here we demonstrate the application of TCP concept for the plasma HHG in the medium allowing the resonance enhancement of single harmonic and those in the vicinity of this maximally enhanced harmonic. Due to the small dispersion of the group velocity in the thin BBO crystal, the temporal overlap of the two pulses (806 and 403 nm) in the plasma region was sufficient for the efficient generation of almost equal odd and even harmonics in the long-wave range of XUV. We analyze

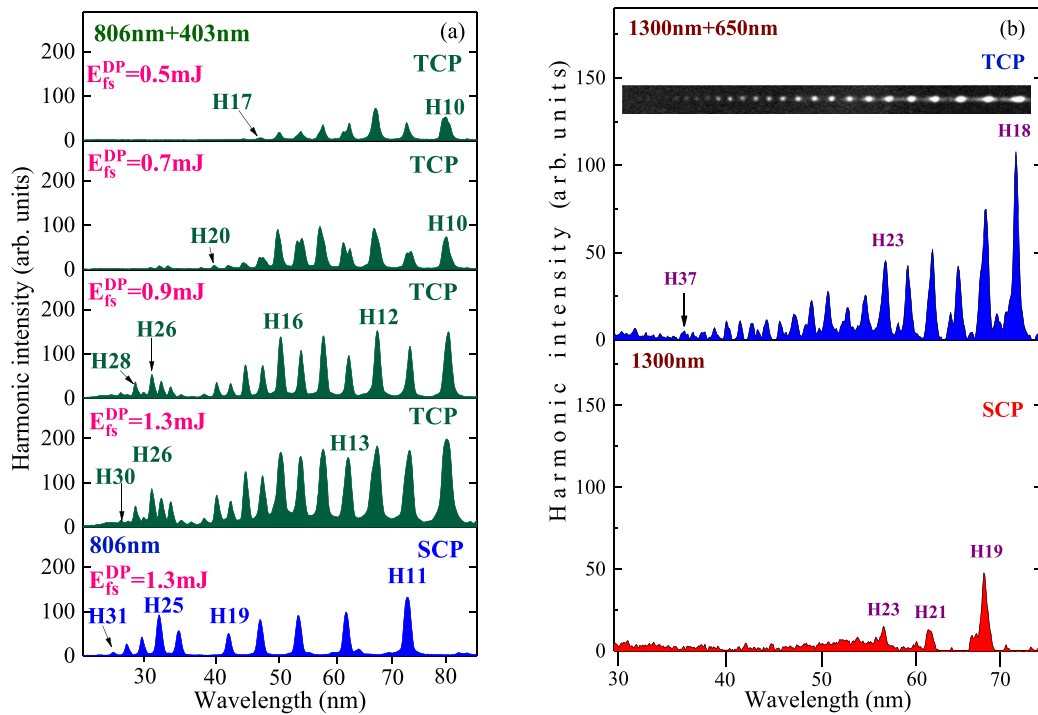


Figure 4. (a) Dependence of harmonic spectra distribution at different energies of the DP at the conditions of TCP of Mo LPP (four upper panels). Bottom panel shows the spectrum obtained in the case of SCP. (b) HHG at the conditions of TCP using 1300 nm pulses and H2 (650 nm) (upper panel). Bottom panel shows the harmonic spectrum using SCP (1300 nm). Inset shows the raw image of saturated harmonics from Mo LPP in the case of TCP (1300 nm + 650 nm).

the effect of this weak second orthogonally polarized field on HHG in Mo plasma at the ratio of the energies of 806 nm and 403 nm pulses $\sim 30:1$.

The role of 806 nm driving pulse energy on the variation and enhancement of harmonics from Mo plasma at the conditions of TCP (806 nm + 403 nm) is shown in figure 4(a). The increase of driving pulse energy from 0.5 to 1.3 mJ caused both the enhancement of conversion efficiency of H2 and the growth of harmonic yield along the whole range of their observation. Notice the appearance of the group of enhanced harmonics with the increase of the energy of DP. The interesting observation is the stronger H26 compared with H25, which demonstrates the optimization of resonance-induced process for the harmonic order, which is better suited to the optimal phase relations between the driving field and even harmonic (H26). The shift of the optimal harmonic order (from H25 towards H26) is clearly seen once one compares two bottom panels of figure 4(a) showing the harmonic spectra in the case of TCP and SCP, respectively.

The application of near-infrared pulses and its second harmonic (1300 nm and 650 nm) for HHG in Mo plasma also demonstrated a significant difference with regard to the SCP [figure 4(b), compare upper and bottom panels]. The gradually decreased odd and even harmonics up to the H37 of the 1300 nm driving radiation were observed (upper panel). Since the cutoff harmonic of this process (H37, $\lambda = 35.1$ nm) lies far from the region of expected resonance enhancement (32 nm), no enhanced harmonics were observed during the experiments using those near-infrared pulses.

Below we show that the resonance enhancement of an individual harmonic can be varied by varying the chirp of driving pulse. This process is based on shifting the harmonic frequencies by changing the chirp of the laser pulse. The laser radiation spectrum remained the same, while the distribution of spectral components along the laser pulses, i.e., the pulse chirp, was modified. The pulse chirp was varied by changing the distance between the gratings of the compressor stage of Ti:sapphire laser. In the case of the positive chirp, the spectrum of the laser radiation was redistributed along the pulse so that its long-wavelength components were moved towards the beginning of the laser pulse and the short-wavelength components dominated in the end of the pulse. The negative chirp corresponded to the inverse distribution of the spectral components. The duration of chirped pulses considerably exceeded the duration of the chirp-free pulses. Since the harmonic generation in the case of high radiation intensities is determined by the leading part of the pulse, the harmonics produced by positively chirped pulses became shifted towards the longer wavelengths with respect to the harmonics generated in the case of chirp-free pulses. Analogously, in the case of negatively chirped pulses, the harmonics shifted to shorter wavelengths since they were generated due to the short-wavelength components of the pulse.

Figure 5(a) shows normalized intensities of three groups of harmonic spectra (H25 and H23). Upper panel demonstrates the almost three-fold enhancement of H25 compared with H23 (see also some panels of figures 2 and 3) in the case of chirp-free DP. Meanwhile, in the case of negatively chirped pulses, which manifests in their larger duration, the spectrum of those

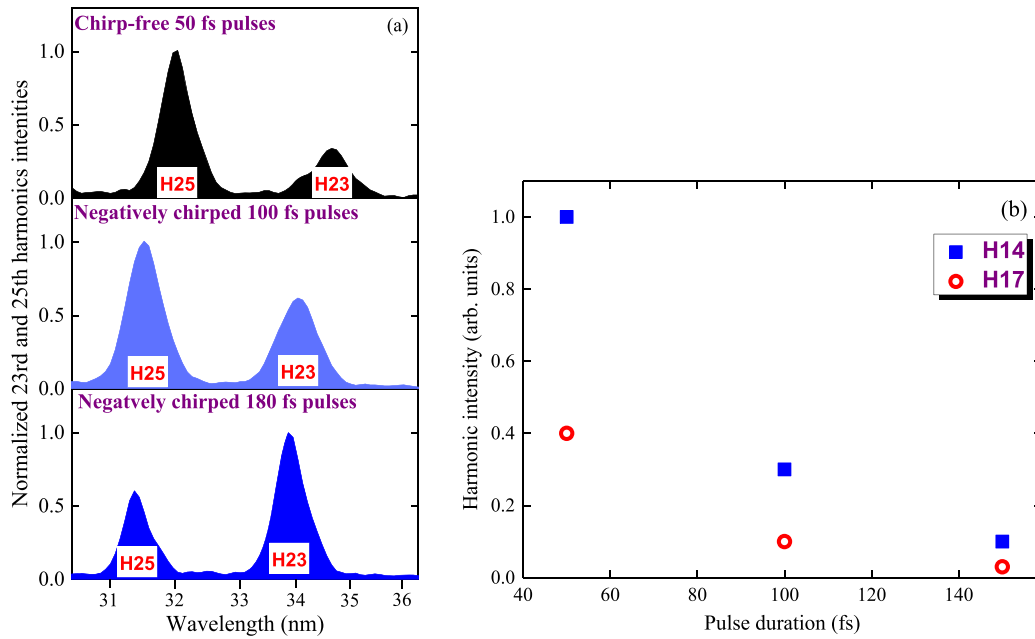


Figure 5. (a) Variation of relative harmonic yields at different negative chirps introduced in the driving pulse in the case of SCP of Mo plasma. (b) Variation of H14 and H17 at different durations of DP using TCP of Mo LPP.

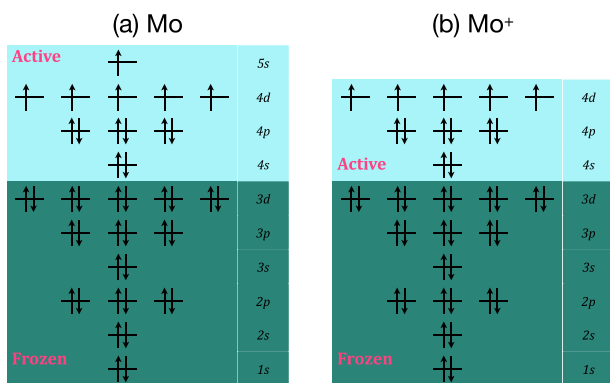


Figure 6. Orbital diagram used in TD-CASSCF calculations for (a) Mo and (b) Mo⁺.

two harmonics was shifted towards the blue side, which caused the detuning of H25 from the ionic resonance of Mo and, correspondingly, optimal resonance-related enhancement. This shift led to variation of the relative intensities of H23 and H25, when, at the 100 fs pulse duration of negatively chirped pulses, their ratio became almost equal to 1 (middle panel). Further introduction of the negative chirp (i.e. using negatively chirped 180 fs DP, bottom panel) caused the prevalence of H23 over H25. This method allows a control of the relative intensity of an individual harmonic with respect to the neighboring ones.

The application of chirped pulses decreases the intensity of laser radiation and leads to corresponding decrease of the harmonic yield. Figure 5(b), shows the strong decrease of H14 and H17 in the case of TCP of Mo plasma using longer pulses. The 3.6 increase of pulse duration (i.e. from 50 to 180 fs) led to the 10-fold decrease of H14 and H17. Such a variation of harmonic yield corroborates with the consideration using the

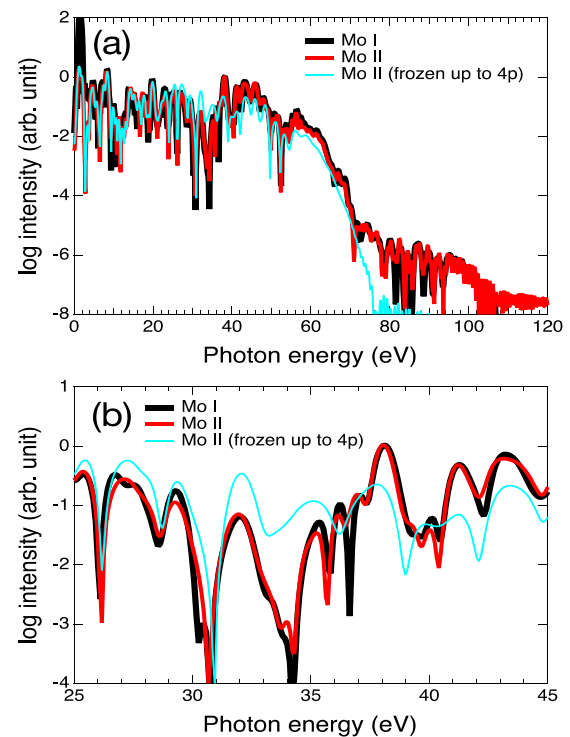


Figure 7. (a) HHG spectra calculated starting from Mo I (black) and Mo II (red). The spectrum for Mo II calculated with frozen core up to 4p (light blue). (b) Close-up.

three-step model predicting the quadratic dependence of the harmonic intensity on the intensity of driving field.

To validate the experimental findings, we numerically simulate HHG from Mo using state-of-the-art implementation of an all-electron three-dimensional real-time *ab initio* method called the time-dependent complete-active-space

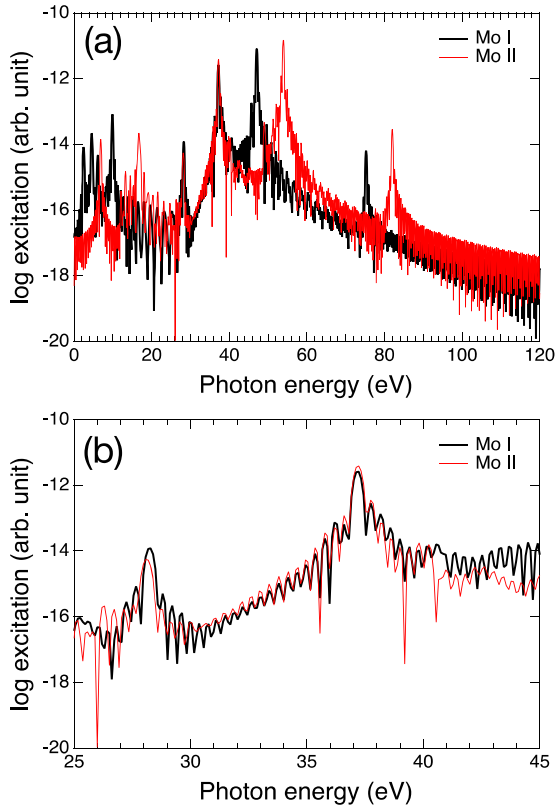


Figure 8. (a) Photoexcitation spectra calculated for Mo I (black) and Mo II (red) as a linear response to a quasi-delta-function pulse. The $1s$ to $3d$ orbitals are treated as dynamical core in these calculations. (b) Close-up.

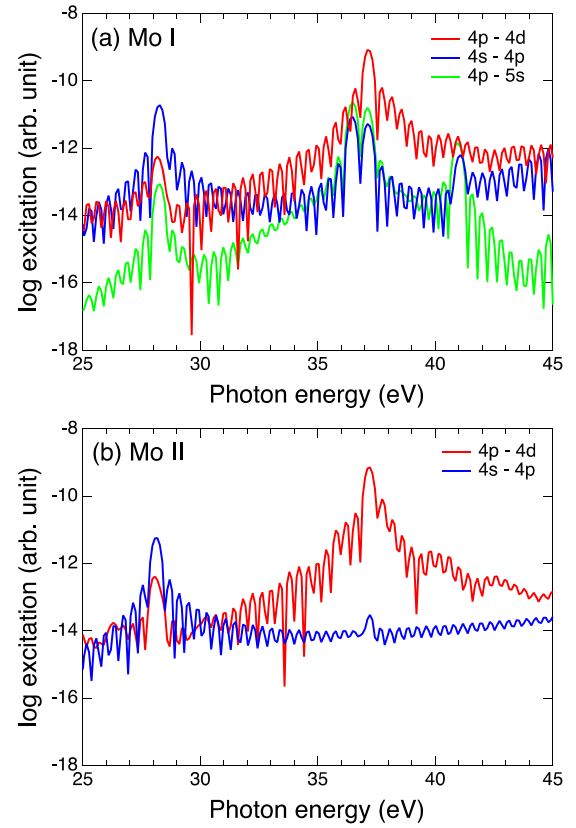


Figure 9. Transition-resolved contributions to photoexcitation spectra (figure 8) for (a) Mo I and (b) Mo II. The vertical scale is not the same as that in figure 8.

self-consistent-field (TD-CASSCF) method [53–57]. In this method, the all-electron total wave function is expressed by the following superposition of Slater determinants consisting of time-dependent spin-orbital functions:

$$\Psi(t) = \hat{A} \left[\Phi_{fc} \Phi_{dc}(t) \sum_I C_I(t) \Phi_I(t) \right] \quad (1)$$

where \hat{A} denotes the antisymmetrization operator, Φ_{fc} and $\Phi_{dc}(t)$ the closed-shell determinants with n_{fc} time-independent doubly-occupied frozen-core and n_{dc} time-dependent doubly-occupied dynamical-core orbitals, respectively. $\{\Phi_I(t)\}$ denote the determinants constructed from n_a active orbitals, among which the active electrons are fully correlated. Previously, this method has been applied to different atoms [54, 57–59], also successfully reproducing resonantly enhanced HHG from Mn and Mn^+ [33]. In this study, specifically, we use orbital subspace decomposition shown in figure 6.

The harmonic spectra obtained for Mo I and Mo II as the initial system for a laser pulse with 806 nm central wavelength, $2 \times 10^{14} \text{ W cm}^{-2}$ peak intensity, and foot-to-foot four-cycle \sin^2 pulse shape are shown in figure 7. The curves for Mo I (black) and Mo II (red) mostly overlap each other, since the neutral Mo is quickly ionized to produce Mo II plasma.

We can see enhancement around 38 eV (32.6 nm, \sim H25) and suppression around 33–34 eV (\sim 36–38 nm, \sim H21–H22),

which well reproduce the experimental features discussed above. In figure 7 is also shown the spectrum calculated for Mo II with up to $4p$ orbitals treated as frozen core in the simulation (light blue). Freezing $4s$ and $4p$ leads to disappearance of both features, which implies that the dynamics of $4s$ and/or $4p$ is relevant with them.

Figure 8 displays the single-photon excitation spectra of Mo I (black) and Mo II (red), obtained as a linear response to a quasi-delta-function pulse [33]. The $1s$ to $3d$ orbitals are treated as dynamical core in these calculations. Both species have a strong excitation around 37 eV. In order to reveal contributions from individual transition lines, let us make a transition-resolved analysis. As detailed in reference [33], we can express a contribution from a transition between orbital pair m and n to the dipole acceleration $\alpha(m, n, t)$ as,

$$\alpha(m, n, t) = 2 \text{Re} \left[\langle m | \hat{f} | n \rangle \langle n | D(t) | m \rangle \right] \quad (2)$$

where $\hat{f} = -Z(\frac{r}{r^3})$ with Z being the atomic number, $D(t)$ denotes the one-electron reduced density matrix, and $\{|n\rangle\}$ the initial orbitals. This analysis serves as a quick convenient estimate, rather than detailed analyses on different atomic transition lines. As we can see from figure 9, which shows the contributions from several orbital pairs, the strong excitation around 37 eV in figure 8 is dominated by the $4p$ - $4d$ resonance. This suggests that the $4p$ - $4d$ transitions are responsible for the HHG enhancement at the similar energy.

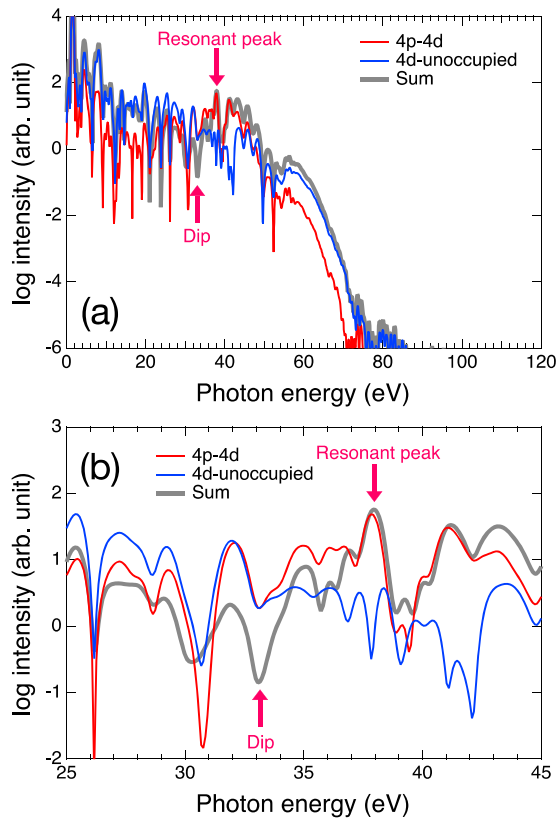


Figure 10. (a) Contribution to HHG in Mo II (figure 7) from the $4p \leftrightarrow 4d$ transitions (red), the transitions between $4d$ and the orbitals initially unoccupied in the Hartree–Fock configuration (blue), and their coherent sum (thick gray). (b) Close-up. The vertical scale is not the same as that in figure 7.

Finally, let us apply the transition-resolved analysis to HHG. The contributions from (i) the transition between $4p$ and $4d$ orbitals (the sum of all the three magnetic quantum numbers), (ii) that between $4d$ and the orbitals initially unoccupied in the Hartree–Fock configuration, and (iii) their coherent sum are displayed in figure 10 for HHG from Mo II (Mo I is quickly ionized to produce Mo II plasma, as discussed above, and the HHG spectrum is dominated by the latter). It should be noted that the present analysis contains the contribution of each inter-orbital transition not only in the ground state but also in different excited and ionized states. We can see that the resonant enhancement around 38 eV is reproduced by (i) the contribution from the $4p$ – $4d$ transitions, while, otherwise, the overall form of the plateau is explained by (ii), i.e., recombination to the $4d$ orbitals (the last step in the three-step model of HHG). Interestingly, the dip around 33–34 eV shows up neither in (i) nor (ii) but in their coherent sum (iii). This observation indicates that the suppression found around 33–34 eV (\sim H21) in both the measured and computed HHG spectra results from the destructive interference between the contributions from the $4p$ – $4d$ transitions and recombination to the $4d$ orbitals.

4. Discussion

There are a few important novelties determined during this research. Firstly, we observed a few enhanced harmonics,

with almost disappeared harmonic order (H21) prior to the amplified group of harmonics (H23–H29), contrary to earlier reported observations of single harmonic. Secondly, we demonstrated the modification of enhancement factor of those harmonics depending on the involvement of different parts of driving pulse spectrum. Thirdly, for the first time to best of our knowledge, the observed enhancement of harmonics was attributed to the involvement of $4p$ – $4d$ transitions of Mo ions in this process, while no reported data in literature were available about the oscillator strengths (gfs) of these transitions. Thus the studies of plasma harmonics from this ablated material allowed demonstrating the prevailing role of some ionic transitions in modification of harmonic spectra distribution from plateau-like to spike-like shape. Moreover, the plasma emission spectra from ablated Mo did not show the presence of those transitions in the vicinity of observed *group of enhanced harmonics* (upper panel of figure 3(b)), while most of previous observations of *single harmonic enhancement* directly attributed this process to already analyzed and reported ionic transitions of some metals with known gfs (Mn, In, As, Sn [34–36]). From these observations, one can deduce the presence of some additional mechanisms of harmonic enhancement in a broader spectral range than a single ionic transition possessing high value of gf . Correspondingly, the four-step model commonly used for classification of such resonance-induced enhanced single harmonic requires additional assumptions to satisfy the observed peculiarities of the enhancement of a group of harmonics. The probable explanation in such behavior of harmonic emission in the vicinity of $4p$ – $4d$ transitions can be attributed to joint involvement of the single-particle related micro-process of single harmonic enhancement and of the multi-particle related macro-process allowing improvement of the phase matching conditions in the vicinity of involved transitions.

All previous studies of the resonant amplification of single harmonics in laser plasmas have shown that this phenomenon is due to a multiphoton resonance with an exceptionally strong transition of a single-charged ion, which can be shifted at some conditions towards certain harmonics of the 800 nm class Ti:sapphire lasers or by using the tunable near-infrared laser sources. This explanation was based solely on the consideration of the single-atom response, leaving aside the collective processes of optimized phase matched conditions in the vicinity of ionic transitions. Our studies show that altered phase matching conditions in the region of anomalous dispersion of a group of ionic transitions can play an important role in explaining the phenomenon of multiple-harmonic amplification and its disappearance at certain conditions. Probably, the combined influence of the processes associated with the involvement of above-mentioned multi-particle and single-particle mechanisms can cause the phenomenon of amplified group of a few harmonics, alongside with single disappeared harmonic. Which of these processes dominates during HHG depends to a certain extent on the specific plasma conditions and the elementary state of the harmonic emitters.

Thus our studies of Mo plasma allowed pointing out the two processes responsible for modification of the envelope of harmonic distribution. Such novelty underlines the advantages

of plasma harmonic research as a tool for the nonlinear optical spectroscopy of ablated species. Particular case of Mo plasma points out the opportunity in determining the group of strong ionic transitions even without knowing their properties from previous spectroscopic studies.

Below we address the characteristics of laser plasma used in our studies. The ionization degree and electron density of Mo plasma were maintained at the conditions when maximal harmonic yield is achieved. Such a control of target ablation allowed achieving the ‘optimal plasma’. This term means the maintenance of such amount of free electrons in plasma when no impeding factors, like phase mismatch between harmonics and driving waves, influence the process of HHG. Correspondingly, ionization degree was not exceeded the conditions when only part of ablated atomic species was ionized. Previous studies of the ablated plasmas from similar targets (density of particles, ionization state, electron density, temperature; for instance in the case of silver [60]) allowed calculating the plasma formation conditions at ‘optimal’ fluence of HP using thermodynamic code HYADES.

Additionally, the particle concentration in the interaction zone can be directly determined by the thermodynamic parameters of the plasma. Note that the heating pulse duration (370 ps) exceeds the characteristic times of electron–phonon (1–10 ps) and electron–electron (~ 10 fs) interactions. The heating laser intensity ($\sim 4 \times 10^9$ W cm $^{-2}$) exceeded a critical intensity corresponding to the threshold for Mo vaporization ($\sim 2 \times 10^9$ W cm $^{-2}$). The absence of an abundance of ionized atoms under such conditions was confirmed by spectral analysis of the plasma. In such a case, the thermal model with gas-dynamics boundary conditions can be applied for the analysis of the formation and heating of laser plasma using various metal targets [61]. Within the framework of this model, the vapor concentration and temperature are determined by the energy and flow conservation laws and saturated vapor concentration. The relation between the surface and the vapor thermal parameters was defined on the basis of the solution of the kinetic equation. Correspondingly, plasma density in the interaction zone was determined to be varied between 5×10^{16} and 2×10^{17} cm $^{-3}$, depending on the plasma sample, experimental conditions, and distance between the target and the driving beam. A similar range of plasma densities was obtained from the calculations using the code HYADES.

Finally, to determine the density one can perform a three-dimensional molecular dynamical simulation of laser ablation of metals using the molecular dynamics code ITAP IMD. The calculations of plasma density at the used experimental conditions of target ablation allow determining this parameter to be $\sim 2.6 \times 10^{17}$ cm $^{-3}$ [16].

The ionization level defined from those studies was varied between 0.3 and 1.3 depending on heating pulse fluence and material of target, while the electron density also changed depending on experimental conditions (3×10^{16} cm $^{-3}$ – 2.5×10^{17} cm $^{-3}$). In present studies, we assumed similar values of plasma densities, ionization state, and electron density when maximal harmonic field was achieved. These thermodynamic

parameters were controlled to some extent through maintaining the optimal plasma formation. Exceeding of above parameters, for instance by increasing the fluence of HP, caused the abrupt decrease of HHG conversion efficiency due to appearance of a large amount of free electrons leading to phase-mismatch of interacting waves, as well as high re-absorption of harmonics and strong plasma emission.

The resonance enhancement can be strongly affected by detuning of the wavelength of DP out from the resonances. The variation of the wavelength of driving femtosecond pulses can be performed by either minor tuning of master oscillators of used lasers, or using the tunable lasers like near infrared OPAs pumped by Ti:sapphire lasers, or applying the chirped pulses from the broadband laser source lasing at a fixed wavelength. The applications of commonly used Ti:sapphire lasers do not offer many opportunities in tuning their wavelength through modification of master oscillators. Nevertheless, in particular cases some minor tuning at around of 800 nm allowed observation of the variations in the enhancement performance of single harmonic, particularly in the case of indium plasma [34]. The broader tuning using OPAs allowed determining the range of driving pulse wavelength at which the resonance enhancement play important role (for instance [62–64]). Meanwhile, simplest method to observe the dynamics of harmonic enhancement is the application of positively or negatively chirped pulses allowing generation of harmonics from either longer- or shorter-wavelength component of the spectrum of DP [65, 66]. In present studies, we applied the latter option to demonstrate the relative variations inside the group of enhanced harmonics. The detuning out from resonances possessing large oscillator strength resulted in decrease of the influence of these resonances on the yield of nearby harmonic. This technique allowed us demonstrating the modification of enhancement factor of those harmonics depending on the involvement of different parts of the driving pulse spectrum (figure 5(a)).

5. Conclusions

In conclusion, we have demonstrated the enhancement of harmonics in the vicinity of 32 nm during HHG in the Mo laser-produced plasma. The enhanced harmonics centered at around of the 25th harmonic of 806 nm radiation have been analyzed by different means (delay between HP and DP, dependences of harmonic yield on the driving and heating pulse intensities and durations, different regimes of plasma formation, TCP of plasma, application of chirped pulses, etc). We discussed the role of strong ionic transition possessing large oscillator strength leading to the growth of the nonlinear optical response. The comparative studies using molybdenum, silver, and chromium laser-produced plasmas are presented.

To validate the experimental findings, we have numerically simulated HHG from Mo using the time-dependent complete-active-space self-consistent-field method. The calculated harmonic spectra have successfully reproduced the presence and position of the experimentally observed enhancement around 32 nm and suppression around 36–38 nm. The single-photon excitation spectra of Mo I and Mo II calculated as a linear response contain a strong excitation at the corresponding

energy (~ 38 eV), dominated by the $4p$ - $4d$ resonance. Our transition-resolved analyses reveal both that the $4p$ - $4d$ transitions are responsible for the observed enhancement and that the destructive interference between the $4p$ - $4d$ transitions and the recombination to the $4d$ orbitals explains the observed suppression.

Acknowledgments

This work was supported by the American University of Sharjah through FRG Grant and the AUS-Common Research Facility. This research was also supported in part by a Grant-in-Aid for Scientific Research from the Ministry of Education, Culture, Sports, Science and Technology (MEXT) of Japan (Grants No. 17K05070, No. 18H03891, and No. 19H00869), JST COI (Grant No. JPMJCE1313), JST CREST (Grant No. JPMJCR15N1), and MEXT Quantum Leap Flagship Program (MEXT Q-LEAP) (Grant No. JPMXS0118067246).

ORCID iDs

I S Wahyutama  <https://orcid.org/0000-0001-5788-4773>

T Sato  <https://orcid.org/0000-0001-8952-7885>

K L Ishikawa  <https://orcid.org/0000-0003-2969-0212>

R A Ganeev  <https://orcid.org/0000-0001-5522-1802>

A S Alnaser  <https://orcid.org/0000-0003-4822-9747>

References

- [1] Vozzi C et al 2005 *Appl. Phys. Lett.* **86** 111121
- [2] Ganeev R A, Redkorechev V I and Usmanov T 1997 *Opt. Commun.* **135** 251
- [3] Ganeev R A et al 2007 *Appl. Phys. B* **87** 243
- [4] Ozaki T, Elouga Bom L B, Ganeev R, Kieffer J-C, Suzuki M and Kuroda H 2007 *Laser Part. Beams* **25** 321
- [5] Ganeev R A 2009 *Phys. Usp.* **52** 55
- [6] Pertot Y, Chen S, Khan S D, Bom L B E, Ozaki T and Chang Z 2012 *J. Phys. B: At. Mol. Opt. Phys.* **45** 074017
- [7] Ganeev R A, Suzuki M, Baba M and Kuroda H 2005 *Appl. Phys. B* **81** 1081
- [8] Singhal H, Naik P A, Kumar M, Chakera J A and Gupta P D 2014 *J. Appl. Phys.* **115** 033104
- [9] Ganeev R A, Suzuki M, Baba M and Kuroda H 2007 *Phys. Rev. A* **76** 023805
- [10] Fareed M A, Thiré N, Mondal S, Schmidt B E, Légaré F and Ozaki T 2016 *Appl. Phys. Lett.* **108** 124104
- [11] Fareed M A, Strelkov V V, Thiré N, Mondal S, Schmidt B E, Légaré F and Ozaki T 2017 *Nat. Commun.* **8** 16061
- [12] Wöstmann M, Splithoff L and Zacharias H 2018 *Opt. Express* **26** 14524
- [13] Abdelrahman Z, Khokhlova M A, Walke D J, Witting T, Zair A, Strelkov V V, Marangos J P and Tisch J W G 2018 *Opt. Express* **26** 15745
- [14] Fareed M A, Strelkov V V, Singh M, Thiré N, Mondal S, Schmidt B E, Légaré F and Ozaki T 2018 *Phys. Rev. Lett.* **121** 023201
- [15] Kumar M, Singhal H and Chakera J A 2019 *J. Appl. Phys.* **125** 155902
- [16] Ganeev R A et al 2012 *Phys. Rev. A* **85** 015807
- [17] Ganeev R A, Suzuki M and Kuroda H 2014 *Phys. Rev. A* **89** 033821
- [18] Ganeev R A, Suzuki M, Baba M, Ichihara M and Kuroda H 2008 *J. Phys. B: At. Mol. Opt. Phys.* **41** 045603
- [19] Ghimire S, DiChiara A D, Sistrunk E, Agostini P, DiMauro L F and Reis D A 2011 *Nat. Phys.* **7** 138
- [20] Toma E S, Antoine P, de Bohan A and Muller H G 1999 *J. Phys. B: At. Mol. Opt. Phys.* **32** 5843
- [21] Bartels R, Backus S, Zeek E, Misoguti L, Vdovin G, Christov I P, Murnane M M and Kapteyn H C 2000 *Nature* **406** 164
- [22] Gaarde M B and Schafer K J 2001 *Phys. Rev. A* **64** 013820
- [23] Zeng Z, Li R, Cheng Y, Yu W and Xu Z 2002 *Phys. Scr.* **66** 321
- [24] Taieb R, Veniard V, Wassaf J and Maquet A 2003 *Phys. Rev. A* **68** 033403
- [25] Milošević D B 2006 *J. Opt. Soc. Am. B* **23** 308
- [26] Milošević D B 2007 *J. Phys. B: At. Mol. Opt. Phys.* **40** 3367
- [27] Milošević D B 2010 *Phys. Rev. A* **81** 023802
- [28] Strelkov V 2010 *Phys. Rev. Lett.* **104** 123901
- [29] Frolov M V, Manakov N L and Starace A F 2010 *Phys. Rev. A* **82** 023424
- [30] Redkin P V and Ganeev R A 2010 *Phys. Rev. A* **81** 063825
- [31] Tudorovskaya M and Lein M 2011 *Phys. Rev. A* **84** 013430
- [32] Redkin P V and Ganeev R A 2017 *J. Phys. B: At. Mol. Opt. Phys.* **50** 185602
- [33] Wahyutama I S, Sato T and Ishikawa K L 2019 *Phys. Rev. A* **99** 063420
- [34] Ganeev R A, Suzuki M, Baba M, Kuroda H and Ozaki T 2006 *Opt. Lett.* **31** 1699
- [35] Suzuki M, Baba M, Kuroda H, Ganeev R A and Ozaki T 2007 *Opt. Express* **15** 1161
- [36] Ganeev R A, Strelkov V V, Hutchison C, Zair A, Kilbane D, Khokhlova M A and Marangos J P 2012 *Phys. Rev. A* **85** 023832
- [37] Abdrabou D, Schneider L M, Rahimi-Iman A, Khedr M A, Hussein A M and El-Sherbini T M 2019 *Plasma Res. Express* **1** 035004
- [38] Ganeev R A 2016 *J. Opt. Soc. Am. B* **33** E93
- [39] Ganeev R A, Kulagin I A, Suzuki M, Baba M and Kuroda H 2005 *Opt. Commun.* **249** 569
- [40] Boltaev G S, Ganeev R A, Kim V V, Zhang K, Venkatesh M and Guo C 2019 *Phys. Plasmas* **26** 100703
- [41] Ganeev R A et al 2006 *J. Opt. Soc. Am. B* **23** 2535
- [42] Ganeev R A 2012 *High-Order Harmonic Generation in Laser Plasma Plumes* (London: World Scientific)
- [43] Kramida A, Ralchenko Y and Reader J NIST ASD Team 2019 NIST atomic spectra database (ver. 5.7.1) <https://doi.org/10.18434/T4W30F>
- [44] Ganeev R A, Suzuki M, Baba M and Kuroda H 2005 *Appl. Phys. Lett.* **86** 131116
- [45] McGuinness C, Martins M, Wernet P, Sonntag B F, van Kampen P, Mosnier J-P, Kennedy E T and Costello J T 1999 *J. Phys. B: At. Mol. Opt. Phys.* **32** L583
- [46] Kim I J, Kim C M, Kim H T, Lee G H, Lee Y S, Park J Y, Cho D J and Nam C H 2005 *Phys. Rev. Lett.* **94** 243901
- [47] Pfeifer T, Gallmann L, Abel M J, Neumark D M and Leone S R 2006 *Opt. Lett.* **31** 975
- [48] Mauritsson J, Johnsson P, Gustafsson E, L'Huillier A, Schafer K J and Gaarde M B 2006 *Phys. Rev. Lett.* **97** 013001
- [49] Charalambidis D, Tzallas P, Benis E P, Skantzakis E, Maravelias G, Nikolopoulos L A A, Conde A P and Tsakiris G D 2008 *New J. Phys.* **10** 025018
- [50] Kim I J, Lee G H, Park S B, Lee Y S, Kim T K, Nam C H, Mocek T and Jakubczak K 2008 *Appl. Phys. Lett.* **92** 021125
- [51] Ganeev R A, Singhal H, Naik P A, Kulagin I A, Redkin P V, Chakera J A, Tayyab M, Khan R A and Gupta P D 2009 *Phys. Rev. A* **80** 033845
- [52] Ganeev R A, Suzuki M and Kuroda H 2014 *Phys. Rev. A* **89** 033821
- [53] Sato T and Ishikawa K L 2013 *Phys. Rev. A* **88** 023402

- [54] Sato T, Ishikawa K L, Březinová I, Lackner F, Nagele S and Burgdörfer J 2016 *Phys. Rev. A* **94** 023405
- [55] Orimo Y, Sato T, Scrinzi A and Ishikawa K L 2018 *Phys. Rev. A* **97** 023423
- [56] Sato T, Orimo Y, Teramura T, Tugs O and Ishikawa K L 2018 *Progress in Ultrafast Intense Laser Science XIV* ed K Yamanouchi, P Martin, M Sentis, L Ruxin and D Normand (Berlin: Springer) p 143
- [57] Orimo Y, Sato T and Ishikawa K L 2019 *Phys. Rev. A* **100** 013419
- [58] Li Y, Sato T and Ishikawa K L 2019 *Phys. Rev. A* **99** 043401
- [59] Orimo Y, Tokesi K, Sato T and Ishikawa K L 2019 *Eur. Phys. J. D* **73** 153
- [60] Elouga Bom L B, Kieffer J-C, Ganeev R A, Suzuki M, Kuroda H and Ozaki T 2007 *Phys. Rev. A* **75** 033804
- [61] Ganeev R A, Elouga Bom L B, Ozaki T and Redkin P V 2007 *J. Opt. Soc. Am. B* **24** 2770
- [62] Ganeev R A, Wang Z, Lan P, Lu P, Suzuki M and Kuroda H 2016 *Phys. Rev. A* **93** 043848
- [63] Ganeev R A, Odžak S, Milošević D B, Suzuki M and Kuroda H 2016 *Laser Phys.* **26** 075401
- [64] Ganeev R A 2017 *J. Appl. Phys.* **121** 133108
- [65] Ganeev R A, Suzuki M, Redkin P V, Baba M and Kuroda H 2007 *Phys. Rev. A* **76** 023832
- [66] Ganeev R A 2016 *Frequency Conversion of Ultrashort Pulses in Extended Laser-Produced Plasmas* (Berlin: Springer)